



Nanometer Precision Time-Stretch Femtosecond Laser Metrology Using Phase Delay Retrieval

Lijie Zhao , Chunbo Zhao, Chuanqing Xia, Zhen Zhang, Tengfei Wu, and Haiyun Xia 

Abstract—A femtosecond laser metrology with nanometer precision and dynamic range of centimeter incorporating time-stretch interferometry and phase delay retrieval method is proposed and experimentally demonstrated. Displacement encoded phase-sensitive temporal interferogram is generated when phase stabilized femtosecond laser pulses transmitting through a time-stretch interferometer. To avoid the chirp of temporal interferogram due to high-order dispersion, time-to-frequency mapping is established to transform the temporal interferogram to the spectral interferogram for high-speed detection. The phase delay of spectral interferogram corresponding to specific displacements is retrieved and accumulated for linear fitting. The fitted slope is the time delay between two arms in the interferometer therefore displacement can be calculated. For precision verification, the preset displacements are measured. Mean error and standard deviation are presented after sliding average of measured results in 4 μ s.

Index Terms—Distance measurement, laser radar, optical interferometry, remote sensing.

I. INTRODUCTION

PRECISE and rapid range measurement is vital for high speed target detection and precise industrial manufacturing, especially in recent years [1], [2]. It is challenging to realize submicron precision at refresh rate of a few mega-hertz. Time-of-flight (TOF) method is widely used in long-range distance measurement [3], [4]. As an example, lidar systems for commercial products such as autonomous vehicles [5] which usually have millimeter precision due to its pulse width and time resolution of acquisition system. To reach higher precision, combined approach based on TOF method and coherent detection is adopted. Cross-correlation-based TOF method [6], [7], synthetic wavelength interferometry [8]–[10], spatial dispersive interferometry [11], [12], and dual comb interferometry

[13]–[15] can realize nanometer precision with averaging time of several milliseconds to seconds.

For pursuing nanometer precision with nanosecond acquisition time, several methods have been proposed. A novel method measures time-of-flight of optical pulse by using electro-optic-sampling-based timing detector (EOS-TD) to compare the timing between femtosecond optical pulse and a frequency-locked periodic electric waveform [16] has been demonstrated recently. In coherent detection, femtosecond laser-based time-stretch technique is another method which has been demonstrated to be feasible, stable and effective in strain measurement [17], [18], ultrafast ranging [19]–[22], imaging [23]–, [25], spectroscopy [26], [27] and microwave photonics applications [28], [29].

Coherent time-stretch technology has revealed its potential to measure dynamic events with rapid variation by extracting displacement from time-domain dispersive interferogram in recent years. In order to eliminate the influence of the chirp of temporal interferogram due to high-order dispersion, time-to-frequency transformation is adopted [30]. The detection speed of time-stretch interferometry is determined by the repetition rate of the femtosecond laser source which is commonly higher than Mega-hertz at communication band. Thus, nanosecond-level acquisition time for capturing single temporal interferogram can be realized which is crucial for high-speed target detection. It has been used in dynamic compression experiments to trace explode debris with tens of kilometers flying speed [31]–[35]. In addition, to deal with problems in massive data storage and real-time signal processing, a method combines time-stretch technique and microwave photonics has been demonstrated [36]. Micrometer precision can be realized in these applications.

In the previous works [19], [36], only the repetition rate of femtosecond laser was locked. The drifted time-domain interferogram on Oscilloscope which indicates the phase shift of the detected signal was observed and this will introduce additional measurement error. This instability originates from the shift of carrier envelope offset (CEO) frequency of the femtosecond laser. It can be precisely controlled by a feedback loop thus the time-domain interferogram can be stabilized [37]–[39]. In [19], the range retrieval method relies on the shape of the femtosecond laser pulse, where the pulse center is retrieved from Gaussian fitting to estimate the time delay value. In fact, the pulse shape in the time-stretch interferometry is difficult to control. Firstly, the pulse envelope is not usually a standard Gaussian. Secondly, the pulse shape is changed due to the inconsistency of the transmission of different optical devices, the unflatness of the gain through amplifiers and the non-uniformity of the

Manuscript received February 10, 2021; revised April 17, 2021; accepted May 7, 2021. Date of publication May 11, 2021; date of current version August 2, 2021. This work was supported in part by the National Key Research and Development (R&D) Plan of China under Grant 2018YFB0504300. (Corresponding author: Haiyun Xia; Tengfei Wu.)

Lijie Zhao, Zhen Zhang, and Haiyun Xia are with the Chinese Academy of Sciences Key Laboratory of Geospace Environment, School of Earth and Space Sciences, University of Science and Technology of China, Hefei, Anhui 230026, China (e-mail: zhaolj@mail.ustc.edu.cn; znzhang@mail.ustc.edu.cn; hsia@ustc.edu.cn).

Chunbo Zhao, Chuanqing Xia, and Tengfei Wu are with the Science and Technology on Metrology and Calibration Laboratory, Changcheng Institute of Metrology and Measurement, Aviation Industry Corporation of China, Beijing 100095, China (e-mail: myy2009zd@163.com; njucqxia@126.com; tengfei.wu@163.com).

Color versions of one or more figures in this article are available at <https://doi.org/10.1109/JLT.2021.3079127>.

Digital Object Identifier 10.1109/JLT.2021.3079127

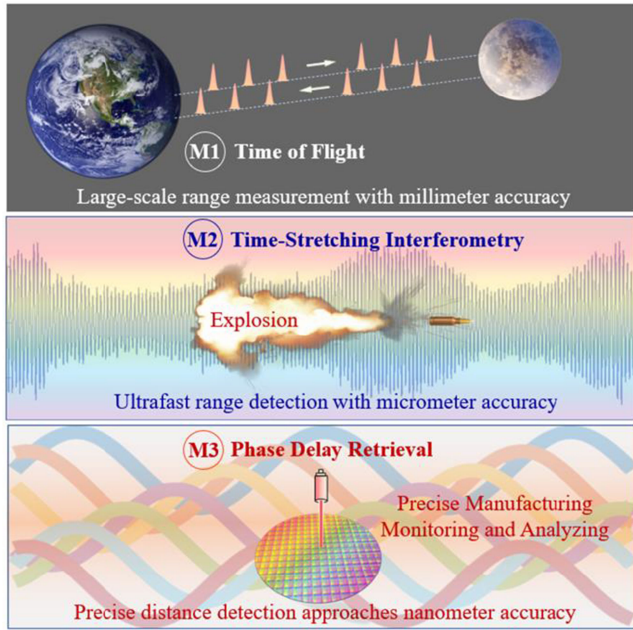


Fig. 1. Precision distance measurement methods and its applications.

response of photodetector. Therefore, we turn to phase retrieval for ranging since it is insensitive to the pulse shape.

Here, we demonstrate a time-stretch ultrafast displacement detection method based on phase detection using femtosecond laser with repetition rate and CEO locking system. Mega-hertz detection speed is realized by dispersive temporal interferometry where a Mach-Zehnder interferometer (MZI) is used and the frequency of the detected signal shifts along with the distance changes. The corresponding displacement can be retrieved through accumulated phase profile by using time-to-frequency mapping with the stabilized time-domain interferogram because the phase change is sensitive to the distance variation. Nanometer precision displacement measurement is realized through single frame captured by high-speed Oscilloscope (OSC) and it has potential to be used for monitoring and analyzing in precise manufacturing. Fig. 1. shows the technical path that we are pursuing to measure distance and displacement with higher precision and its possible applications.

II. PRINCIPLE

The system schematic diagram of the phase sensitive time-stretch laser metrology is shown in Fig. 2. The phase delay profile is retrieved by time-stretch interferometry through a phase-stabilized femtosecond laser for displacement measurement.

A. Phase-Stabilized Femtosecond Laser Source

As shown in the upper part of Fig. 2, the optical source is a homemade femtosecond laser (FSL), with its repetition rate and carrier envelope offset frequency locked via closed-loop control. The oscillator of femtosecond laser is comprised of 980 nm pump source and a “6-shape” cavity which contains Er-doped fiber, wavelength division multiplexer (WDM), fiber

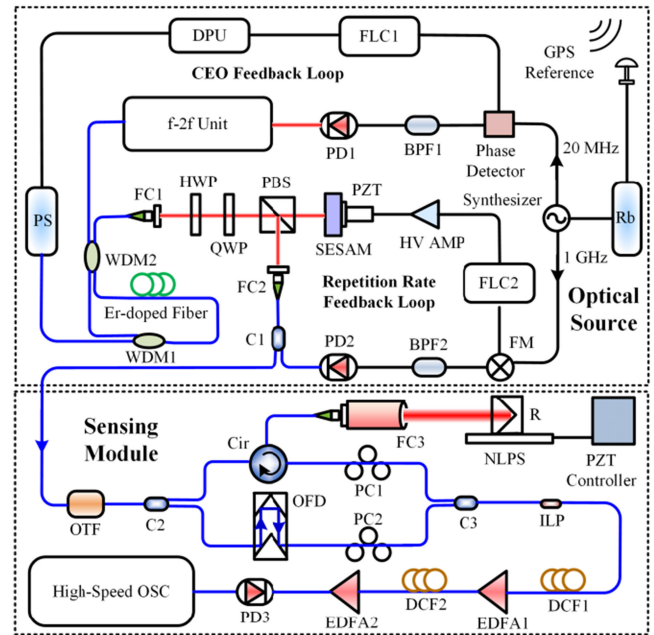


Fig. 2. Schematic diagram of time-stretch femtosecond laser metrology. PS: Pump source; WDM: Wavelength division multiplexer; FC: Fiber collimator; HWP: Half-wave plate; QWP: Quarter-wave plate; PBS: Polarization beam splitter; C: Coupler; PD: Photodetector; SESAM: Semiconductor saturable absorption mirror; PZT: Piezo-electric transducer; BPF: Band-pass filter; FM: Frequency mixer; FLC: Feedback loop controller; HV AMP: High-voltage amplifier; Rb: Rubidium clock; DPU: Driving power unit; OTF: Optical tunable filter; Cir: Circulator; PC: Polarization controller; ILP: In-line polarizer; OFD: Optical fiber delayer; R: Retroreflector mirror; NLPS: Nanometer linear position stage; DCF: Dispersion compensation fiber; EDFA: Erbium-doped fiber amplifier; OSC: Oscilloscope.

collimator (FC), half-wave plate (HWP), quarter-wave plate (QWP), polarization beam splitter (PBS) and a semiconductor saturable absorption mirror (SESAM). The SESAM is stick to a piezo-electric transducer (PZT) to control the cavity length. The femtosecond laser is split by a PBS from the cavity, then coupled to a fiber coupler in which one part is used for output and the other part is used for repetition rate locking (RRL).

In the RRL process, the femtosecond laser pulses are detected by a photodetector (PD2), the high-order harmonics are included in the output signal and can be selected by a bandpass filter (BPF2). The selected high-order harmonic is combined at a frequency mixer (FM) together with a reference signal to generate a difference frequency signal which can reflect the fluctuation of the repetition rate. The difference frequency signal is then sent to a feedback loop controller (FLC2) which is a proportional-integral (PI) controller. The control signal of the PZT is output from FLC and amplified by a high-voltage amplifier (HV AMP). The PZT adjusts the cavity length until balanced state is achieved and the high-order harmonic is synchronized with the reference signal. Thus, the higher stability of the repetition frequency can be reached.

Another portion of light split from the cavity through WDM2 is used for CEO frequency locking. The CEO frequency can be obtained by detecting the beat signal from an f-2f self-referencing system [40], [41]. In the f-2f unit, the spectrum is expanded by high-nonlinear fiber, followed by a PPLN crystal

and a diffraction grating for beat signal selection. Then the beat signal is filtered by BPF1 as the CEO locking signal. A digital phase-frequency detector is used to obtain the difference frequency signal of the CEO locking signal and its reference signal. The difference frequency signal is sent to FLC1 to generate control signal for adjusting pump source current through the driving power unit (DPU). The pump power can be altered to change the CEO frequency of femtosecond laser until balanced state is achieved during the oscillation adjustment process therefore the CEO frequency is synchronized with the reference signal.

The reference signals in the locking processes of repetition rate and CEO frequency are output from a frequency synthesizer which is external-referenced to a GPS-referenced Rubidium (Rb) clock. Thus, the repetition rate and the CEO frequency signal have the same frequency stability of the Rb clock and the phase stabilized femtosecond laser is realized.

B. Time-Stretch Interferometry

As shown in the lower part of Fig. 2, the displacement measurement is based on time-stretch (dispersive Fourier transformation) interferometry [19], [20]. The output femtosecond laser is sent to the sensing module. Only a portion of few nanometer of the whole spectrum of the femtosecond laser is filtered and sent to a Mach-Zehnder Interferometer. Note that, a femtosecond laser may have a wide spectrum over one hundred nanometers, multi-channel ranging system can be realized conveniently by wavelength division multiplexing technique. Here, the filtered pulse is time-stretched by two spool of dispersion compensation fiber (DCF) and amplified by two Erbium-doped fiber amplifiers (EDFA) in cascade. The time-domain interferogram is detected by a fast photodetector and sampled by a high-speed Oscilloscope. The displacement under test is controlled by a nanometer linear positioning stage (NLPS).

In the first step, the distance between two arms of MZI is encoded in the temporal interferogram by dispersive Fourier transformation using DCF. The temporal interferogram is chirped due to high-order dispersion. It can be expressed by [19]:

$$I_{TI}(t) = I_t(t) [1 + \cos(\omega_t t)] \quad (1)$$

where $I_t(t)$ is the temporal envelope and ω_t is the chirped angular frequency. If the third-order dispersion is considered ω_t can be written as [36]:

$$\omega_t = \frac{\tau}{\beta_2 L} - \frac{\beta_3 L \tau^2}{2(\beta_2 L)^3} - \frac{\beta_3 L \tau t}{(\beta_2 L)^3} \quad (2)$$

where τ is the time delay between the two arms of MZI, β_2 , β_3 and L are the second-order, third-order dispersion coefficient and length of the DCF. It is difficult to obtain time delay value by multi-parameter curve fitting without knowing the exact dispersion coefficient. Here, direct temporal analysis is not adopted.

From the other view in the frequency-domain, the interferogram can be expressed by:

$$I_{FI}(\omega) = I_f(\omega) [1 + \cos(\omega \tau)] \quad (3)$$

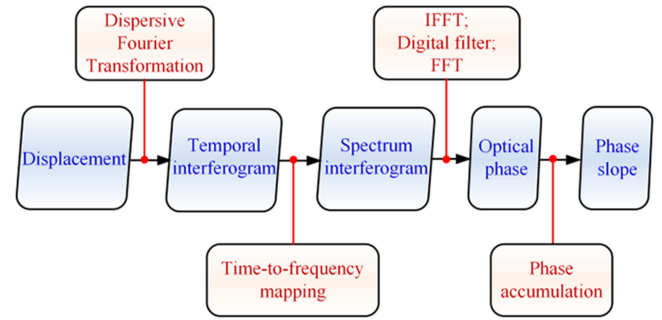


Fig. 3. Flow chart of the displacement measurement based on accumulated phase.

where $I_f(\omega)$ is the spectrum envelope and ω is the optical angular frequency. It is shown that the spectral interferogram is non-chirped and can be expediently manipulated.

C. Time-to-Frequency Mapping and Phase Delay Retrieval

In order to obtain the corresponding spectral interferogram, in the second step, time-to-frequency mapping is used. The temporal and spectral interferograms can be measured simultaneously by OSC and OSA respectively at a specific distance. Thus, the time-to-frequency mapping of the system can be uniquely established by polynomial fitting. The spectral interferogram of different distance can be directly obtained by the calibrated mapping function.

In the third step, the spectral interferogram is resampled uniformly by using cubic spline interpolation. For accurate phase retrieval, the inverse fast Fourier transformation (IFFT) is applied to the resampled spectral interferogram firstly and a digital bandpass filter is then applied to eliminate the temporal direct current component. The phase value with the range from $-\pi$ to π in frequency domain is then obtained by fast Fourier transformation (FFT).

In the final step, the optical phase can be accumulated by phase delay retrieval algorithm [42], [43]. According to (3), the phase of the spectral interferogram has linear relationship relative to the frequency. The time delay τ can be simply obtained which is the linear fitting slope of the accumulated phase. For a reference position R and a target position D to be measured, the displacement between the two positions can be written as:

$$d_{TBD} = c(s_D - s_R)/2 \quad (4)$$

where s_R and s_D are the slope of the reference and target position, c is the speed of the light.

The flow chart of the principle of the displacement measurement based on accumulated phase delay retrieval is shown in Fig. 3. The measurement process is simple and straightforward.

The drift of the temporal interferogram with displacement relative to reference point is shown clearly in Fig. 4. The two reference points R1 and R2 are selected. R1 is set at displacement of 0 μm which is the zero point of NLPS and R2 is set at displacement of 2000 μm from R1, moving distance Δd is 0.2 μm . The phase of the temporal interferogram is sensitive to the

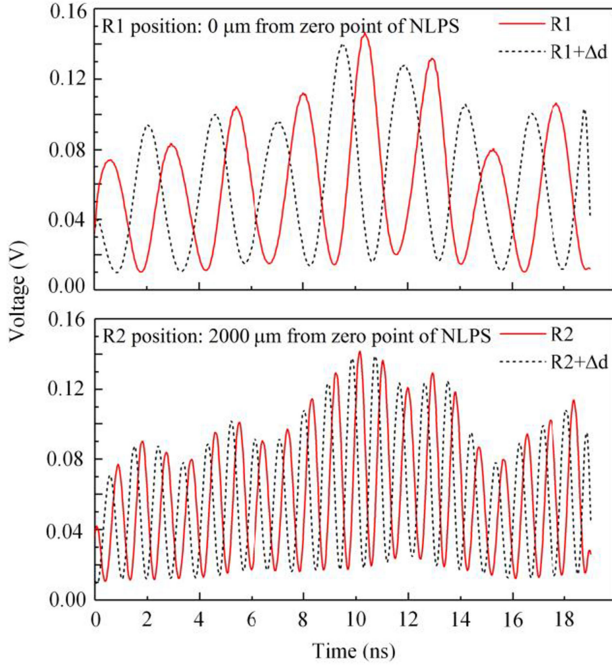


Fig. 4. Temporal interferogram drift with a specific displacement relative to reference points ($\Delta d = 0.2\mu\text{m}$).

displacement when the repetition rate and CEO frequency are locked.

The dynamic range of the system is $r_d = |DL\lambda^2\Delta f/2|$, where D is the dispersion coefficient and λ is the center wavelength. Δf is the Optical-Electro (OE) bandwidth of the system. In this work, $DL = -2298$ ps/nm, the OE bandwidth is 25 GHz which is the lower value of the PD3 (Alphas, UPD-15-IR2-FC, 25 GHz bandwidth) and the OSC (Teledyne Lecroy, LabMaster-10-Zi, 36 GHz bandwidth) thus the dynamic range is 69.9 nm.

III. EXPERIMENT AND DISCUSSION

In the experiment, the homemade femtosecond laser (CIMM, TC1550-2G) has average output power of 30 mW and pulse width of about 93 fs. A 980 nm laser source (connet, VLSS-980-M) is used as the pump. The repetition rate is designed to be 50 MHz, the locking frequency is selected to be the 20-order harmonics which is 1 GHz to ensure the basic harmonic locking stability. The CEO locking frequency is set to be 20 MHz. The reference signals for repetition rate and CEO frequency feedback loops generated by the synthesizer are set accordingly. The synthesizer is GPS-referenced by a Rb clock (Microsemi, 8040C) for high precision. In the CEO feedback loop, the f_{CEO} signal is detected by PD1 (Thorlabs, APD110C/M) and then controlled by FLC1 (Menlosystem, SYNCRO-CEO). In the repetition rate feedback loop, f_{rep} signal is detected by PD2 (EOT, ET-3000A) and then controlled by FLC2 which is a homemade proportional-integral controller and the output is connected to a PZT controller with high-voltage amplifier (COREMORROW, E52) to adjust the laser cavity length. f_{rep} and f_{CEO} are monitored by an OSC (RIGOL, DS1104) and an electric spectrum analyzer (RIGOL, DSA815) respectively. The laser absolute frequency fluctuation

TABLE I
SUMMARY OF SYSTEM PARAMETERS

Parameters	Values
Optical Source:	
Femtosecond laser:	
Center wavelength	1560 nm
Repetition rate	50 MHz
CEO frequency	20 MHz
Pulse width	93 fs
Average power	30 mW
Sensing Module:	
Collimated beam diameter	3.6 mm
Total dispersion of DCF	-2298 ps/nm
Bidirectional repeatability of NLPS	50 nm
Bandwidth of PD3	25 GHz

TABLE II
COEFFICIENT OF CALIBRATED TIME-TO-FREQUENCY MAPPING

Equation	$y = at + bt^2 + ct^3 + d$
a	5.04007×10^{19}
b	-3.92690×10^{25}
c	5.72828×10^{33}
d	1.91699×10^{14}

is detected by a frequency counter (KEYSIGHT, 53220A) and 30 Hz fluctuation is observed during 100 seconds.

In the sensing module, optical filter bandwidth is 7.5 nm with wavelength center at 1560 nm. The diameter of the beam collimated on the retroreflector is 3.6 mm. The retroreflector is placed on a PZT-driving NLPS (PI, N-565.260) with bidirectional repeatability of 50 nm and placed it at a distance of 25 cm from the collimator. The dispersion of DCF (ofs, DCM(D)-C-G.652-DCF) used in the system is -2298 ps/nm. The EDFAs are adjusted to ensure the proper signal to noise ratio (SNR). The temporal interferogram is detected by an In-GaAs ultrafast photodetector (Alphas, UPD-15-IR2-FC) and sampled by a high-speed OSC (Teledyne Lecroy, LabMaster MCM-Zi-A) with 36 GHz bandwidth and high sampling rate up to 80 GSa/s. The spectral interferogram is measured by an OSA (Yokogawa, AQ6370C). The basic system parameters are shown in TABLE I.

All the fiber devices are placed in a temperature-controlled box and settled on an air-floating platform for stable environment during the measurements.

The time-to-frequency mapping is obtained by matching the local maximums of temporal and spectral interferogram using 3rd-order polynomial curve fitting to calibrate high-order dispersion of DCF. The entire system is calibrated by the mapping function and no adjustment is needed during the measurement. During the interferogram acquisition for the calibration, the resolution of OSA is 0.02 nm, the sampling rate and average times of OSC are set as 40 GSa/s and 1000. The mapping equation and coefficients are shown in TABLE II. The time t is in the range of 0-20 ns according to the pulse period.

The measurement reference point R is chosen to be the zero point of the NLPS which is the middle point in its travel range. Several displacements are selected for experimental verification.

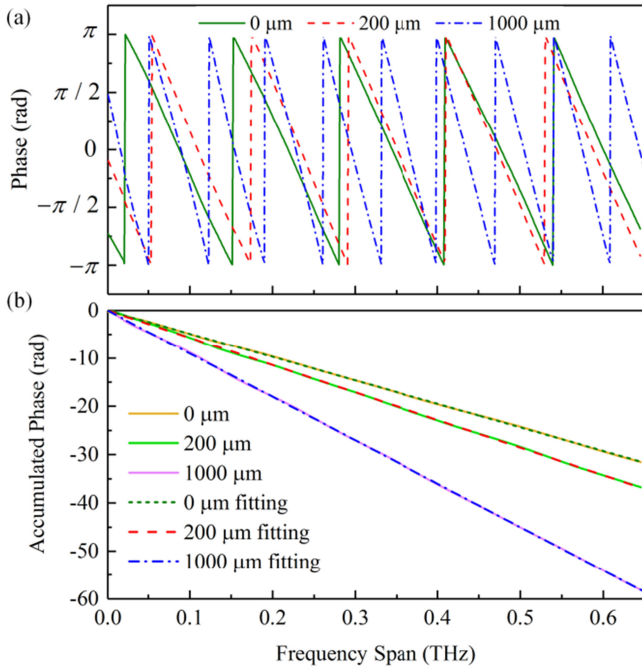


Fig. 5. Phase and accumulated phase of different displacements.

With the calibrated time-to-frequency mapping function. The temporal interferogram is directly transformed to spectral interferogram. 6.5 THz frequency range around the middle of spectral interferogram is picked out for phase retrieval.

Zero point, 200 μm and 1000 μm positions are selected to show the process of phase retrieval for clarity. In one single measurement, the measured phase is shown in Fig. 5(a). With femtosecond laser absolute frequency locked, the phase profile is stable without temporal drifting. The frequency increases when the displacement increases relative to the reference point and the phase slope is steeper with longer displacement.

The accumulated phase and linear fitting lines are shown in Fig. 5(b). The accumulated phase of the spectral interferogram is obtained by the phase retrieval algorithm [42], [43]. Note that, the origin of the fitting line is shifted to zero to emphasize the relation between the fitting slope and displacements. The fitting slope is the time delay τ between the two arms of MZI in the sensing module. The time delay between target position and reference point is obtained by slope difference $S_D - S_R$. Thus, the displacement can be calculated by (4).

To assess the precision with achievable averaging time of the system, Allan deviation at 1000 μm and 5000 μm displacement is measured with sampling rate of 40 GSa/s as shown in Fig. 6. Considering the limitation of high-speed data storage capability at high sampling rate of the OSC used in this work, the total acquisition time is set to 480 μs which corresponds to 24000 single pulses. It is shown that the Allan deviation can be reduced less than 100 nm with averaging time of microsecond-level for 5000 μm displacement. The Allan deviation increases along with larger displacement is due to the frequency of the temporal interferogram increases and the number of sampling points is reduced in single interference fringe. Thus, the accuracy of phase retrieval is degraded.

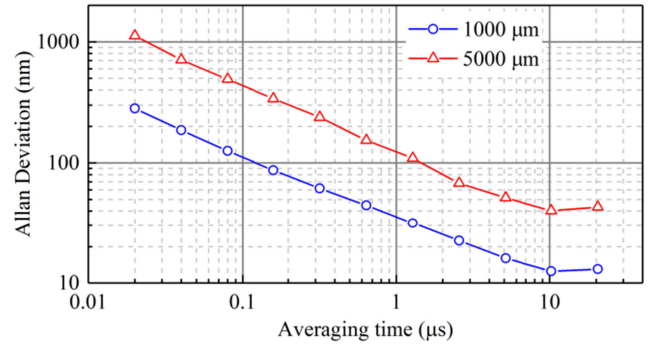


Fig. 6. Allan deviation versus averaging time at 1000 μm and 5000 μm displacement with sampling rate of 40 GSa/s.

Since the target to be measured is static, sliding averaging of measured results from each single pulse is adopted for higher robustness, meanwhile, lightening the burden of data acquisition and storage. The sliding window is set to 50 measured distance sequence which corresponds to 1 μs and the sliding step is set to 1 measured distance which corresponds to 20 ns. The results of preset displacements after sliding averaging are shown in Fig. 7. There are 150 points which correspond to total acquisition time of 3.98 μs for each displacement. The sampling rate is set to be 20 GSa/s for 200 μm , 40 GSa/s for 1000 μm and 5000 μm and 80 GSa/s for 10000 μm displacement respectively for precise phase retrieval. At 200 μm displacement, the mean error is -34.2 nm with standard deviation of 28.5 nm. At 1000 μm displacement, the mean error is -21.6 nm with standard deviation of 31.0 nm. At 5000 μm , the mean error is 23.0 nm with standard deviation of 84.6 nm. At 10000 μm , the mean error is -2.3 nm with standard deviation of 175.2 nm. As is revealed in Allan deviation measurement above, the increase of the standard deviation is also observed for the same reason.

In the experiment, because of the accumulated phase of spectral interferogram is used for displacement retrieval, larger spectral bandwidth selection with the same dispersion of femtosecond pulses can provide more sampling points for linear fitting which can enhance the fitting accuracy. For larger displacement, normalization and sinusoidal fitting of spectral interferogram after time-to-frequency mapping can improve the measurement performance. During the measurements, the measured displacement precision is affected by the time jitter of OSC and the flatness of retroreflector mirror since collimated light beam with diameter of 3.6 mm is used in this work. The NLPS is mechanically connected on a manually controlled positioning stage with 150 mm travel range for coarse position adjustment. Therefore, temperature fluctuation of the environment and strain variation during the movement of the NLPS are possible to influence the measured mean value. In addition, the measured mean value can also be affected by the NLPS, since its bidirectional repeatability declared by the manufacturer is 50 nm.

IV. CONCLUSION

A femtosecond laser metrology with centimeter-dynamic range for displacement detection incorporating time-stretch technique and phase delay retrieval algorithm is proposed and

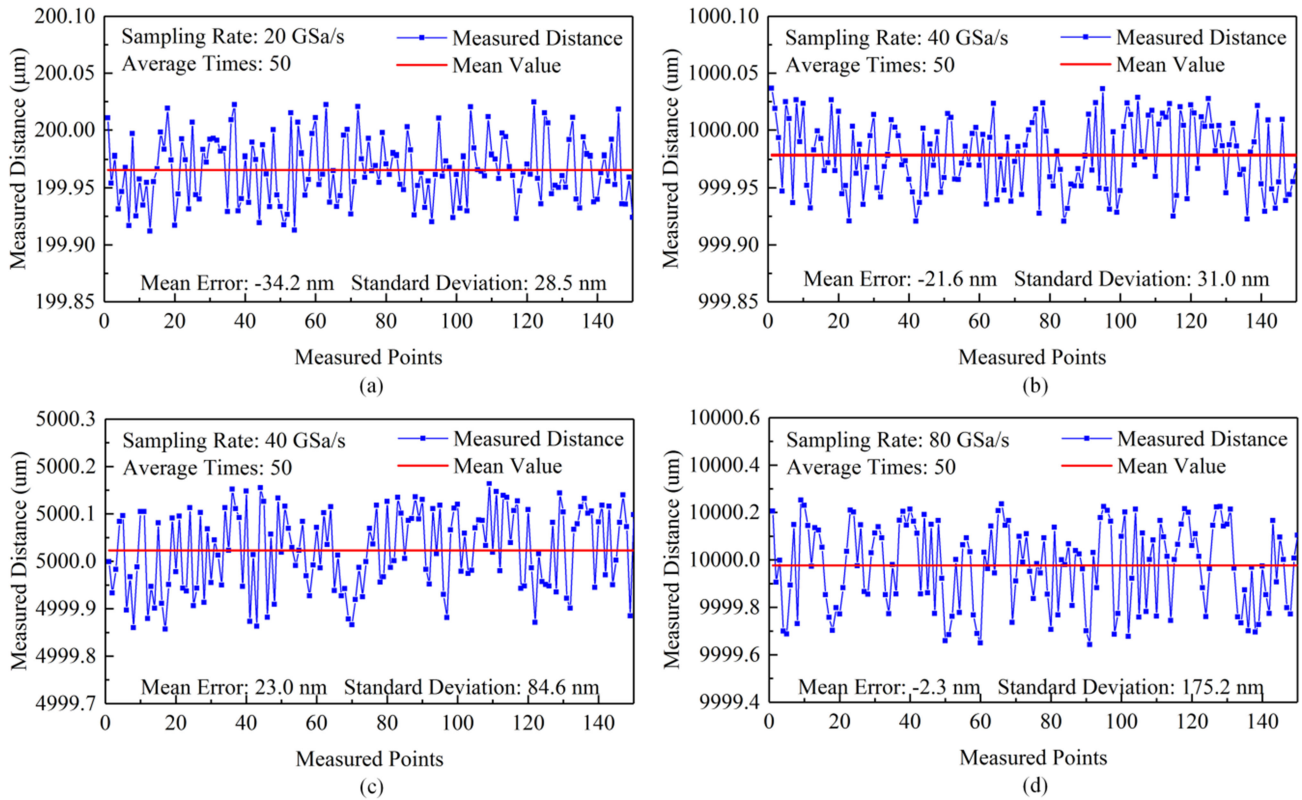


Fig. 7. (a) 200 μm displacement measured results. (b) 1000 μm displacement measured results. (c) 5000 μm displacement measured results. (d) 10000 μm displacement measured result.

demonstrated. The previous signal processing method [19] relies on the shape of the femtosecond laser pulse which is difficult to control because it can be altered in dispersion, amplification and detection process, whereas the new method in this work is insensitive to the pulse shape and the precision is enhanced. With repetition rate and carrier envelope offset frequency locked by two feedback loops, stable temporal interferograms are obtained and then transformed to the spectral interferogram by time-to-frequency mapping for fast detection. Displacement is simply retrieved from the linear fitting slope of the accumulated phase delay. The system has the potential to be used for fast dynamic event detection and precise high-speed imaging. Larger dynamic range can be realized by combining other method such as TOF and synthetic wavelength method.

REFERENCES

- [1] R. Teti, K. Jemielniak, G. O'Donnell, and D. Dornfeld, "Advanced monitoring of machining operations," *CIRP Annu. Manuf. Technol.*, vol. 59, no. 2, pp. 717–739, Jul. 2010.
- [2] A. Fleming, "A review of nanometer resolution position sensors: Operation and performance," *Sensor Actuators A-Phys.*, vol. 190, pp. 106–126, Feb. 2013.
- [3] T. Murphy *et al.*, "APOLLO: Millimeter lunar laser ranging," *Classical Quantum Gravity*, vol. 29, no. 18, Aug. 2012, Art. no. 184005.
- [4] A. McCarthy *et al.*, "Kilometer-range, high resolution depth imaging via 1560 nm wavelength single-photon detection," *Opt. Exp.*, vol. 21, no. 7, pp. 8904–8915, Apr. 2013.
- [5] J. Liu, Q. Sun, Z. Fan, and Y. Jia, "TOF lidar development in autonomous vehicle," in *Proc. IEEE 3rd Optoelectron. Glob. Conf.*, Shenzhen, China, Sep. 2018, pp. 185–190.
- [6] J. Ye, "Absolute measurement of a long, arbitrary distance to less than an optical fringe," *Opt. Lett.*, vol. 29, no. 10, pp. 1153–1155, May 2004.
- [7] J. Lee, Y. J. Lim, K. Lee, S. Lee, and S. W. Kim, "Time-of-flight measurement with femtosecond light pulses," *Nat. Photon.*, vol. 4, pp. 716–720, Aug. 2010.
- [8] G. Wu, L. Liao, S. Xiong, G. Li, Z. Cai, and Z. Zhu, "Synthetic wavelength interferometry of an optical frequency comb for absolute distance measurement," *Sci. Rep.*, vol. 8, Mar. 2018, Art. no. 4362.
- [9] Y. Jang *et al.*, "Comb-referenced laser distance interferometer for industrial nanotechnology," *Sci. Rep.*, vol. 6, Aug. 2016, Art. no. 31770.
- [10] Z. Zhu, G. Xu, K. Ni, Q. Zhou, and G. Wu, "Synthetic-wavelength-based dual-comb interferometry for fast and precise absolute distance measurement," *Opt. Exp.*, vol. 26, no. 5, pp. 5747–5757, Mar. 2018.
- [11] I. Coddington, W. C. Swann, L. Nenadovic, and N. R. Newbury, "Rapid and precise absolute distance measurements at long range," *Nat. Photon.*, vol. 3, pp. 351–356, May 2009.
- [12] J. Wang *et al.*, "Long-distance ranging with high precision using a soliton microcomb," *Photon. Res.*, vol. 8, no. 12, pp. 1964–1972, Dec. 2020.
- [13] T. Liu, N. Newbury, and I. Coddington, "Sub-micron absolute distance measurements in sub-millisecond times with dual free-running femtosecond fiber-lasers," *Opt. Exp.*, vol. 19, no. 19, pp. 18501–18509, Sep. 2011.
- [14] H. Zhang, H. Wei, X. Wu, H. Yang, and Y. Li, "Absolute distance measurement asynchronous optical sampling," *Opt. Exp.*, vol. 22, no. 6, pp. 6597–6604, Mar. 2014.
- [15] S. Zhou, C. Lin, Y. Yang, and G. Wu, "Multi-pulse sampling dual-comb ranging method," *Opt. Exp.*, vol. 28, no. 3, pp. 4058–4066, Feb. 2020.
- [16] Y. Na *et al.*, "Ultrafast, sub-nanometre-precision and multifunctional time-of-flight detection," *Nat. Photon.*, vol. 14, pp. 355–360, Jun. 2020.
- [17] E. J. Ahmad, C. Wang, D. Feng, Z. Yan, and L. Zhang, "High temporal and spatial resolution distributed fiber Bragg grating sensors using time-stretch frequency-domain reflectometry," *J. Lightw. Technol.*, vol. 35, no. 16, pp. 3289–3295, Aug. 2017.
- [18] S. Gilbertson *et al.*, "High speed, localized multi-point strain measurements on a containment vessel at 1.7 MHz using swept-wavelength laser-interrogated fiber Bragg gratings," *Sensors*, vol. 20, Oct. 2020, Art. no. 5935.

- [19] H. Xia and C. Zhang, "Ultrafast ranging lidar based on real-time Fourier transformation," *Opt. Lett.*, vol. 34, no. 14, pp. 2108–2110, Jul. 2009.
- [20] H. Xia and C. Zhang, "Ultrafast and Doppler-free femtosecond optical ranging based on dispersive frequency modulated interferometry," *Opt. Exp.*, vol. 18, no. 5, pp. 4118–4129, Mar. 2010.
- [21] B. M. La Lone, B. R. Marshall, E. K. Miller, G. D. Stevens, W. D. Turley, and L. R. Veeger, "Simultaneous broadband laser ranging and photonic doppler velocimetry for dynamic compression experiments," *Rev. Sci. Instrum.*, vol. 86, no. 2, Feb. 2015, Art. no. 023112.
- [22] J. Wang *et al.*, "Multi-reference broadband laser ranging to increase the measuring range," *Rev. Sci. Instrum.*, vol. 90, no. 3, Mar. 2019, Art. no. 033108.
- [23] K. Goda, K. K. Tsia, and B. Jalali, "Serial time-encoded amplified imaging for real-time observation of fast dynamic phenomena," *Nature*, vol. 458, pp. 1145–1149, Apr. 2009, Art. no. 07980.
- [24] J. Jiang, S. Karpf, and B. Jalali, "Time-stretch LiDAR as a spectrally scanned time-of-flight ranging camera," *Nat. Photon.*, vol. 14, pp. 14–18, Jan. 2020.
- [25] G. Wang, Z. Yan, L. Yang, L. Zhang, and C. Wang, "Improved resolution optical time stretch imaging based on high efficiency in-fiber diffraction," *Sci. Rep.*, vol. 8, Jan. 2018, Art. no. 600.
- [26] J. Chou, D. R. Solli, and B. Jalali, "Real-time spectroscopy with subgigahertz resolution using amplified dispersive fourier transformation," *Appl. Phys. Lett.*, vol. 92, no. 11, Feb. 2008, Art. no. 111102.
- [27] Z. Zhang, H. Xia, S. Yu, L. Zhao, T. Wei, and M. Li, "Femtosecond imbalanced time-stretch spectroscopy for ultrafast gas detection," *Appl. Phys. Lett.*, vol. 116, no. 17, Apr. 2020, Art. no. 171106.
- [28] C. Wang, "Dispersive Fourier transformation for versatile microwave photonics applications," *Photonics*, vol. 1, pp. 586–612, Dec. 2014.
- [29] X. Zou, B. Lu, W. Pan, L. Yan, A. Stöhr, and J. Yao, "Photonics for microwave measurements," *Laser Photon. Rev.*, vol. 10, no. 5, pp. 711–734, Jul. 2016.
- [30] H. Xia, C. Wang, S. Blais, and J. Yao, "Ultrafast and precise interrogation of fiber Bragg grating sensor based on wavelength-to-time mapping incorporating higher order dispersion," *J. Lightw. Technol.*, vol. 28, no. 3, pp. 254–261, Feb. 2010.
- [31] C. V. Bennett *et al.*, "Broadband laser ranging development at the DOE labs," *Proc. SPIE*, San Francisco, CA, USA, vol. 10089, Feb. 2017, Art. no. 100890F.
- [32] N. Kostinski *et al.*, "Broadband laser ranging: Signal analysis and interpretation," *Proc. SPIE*, San Francisco, CA, USA, vol. 10089, Feb. 2017, Art. no. 100890G.
- [33] M. Rhodes, C. Bennett, and D. Perry, "Accuracy and precision in broadband laser ranging," *Proc. SPIE*, San Francisco, CA, USA, vol. 10517, Feb. 2018, Art. no. 105170B.
- [34] M. Rhodes *et al.*, "Validating data analysis of broadband laser ranging," *Rev. Sci. Instrum.*, vol. 89, no. 3, Mar. 2018, Art. no. 035111.
- [35] J. G. Mance, B. M. La Lone, D. H. Dolan, S. L. Payne, D. L. Ramsey, and L. R. Veeger, "Time-stretched photonic Doppler velocimetry," *Opt. Exp.*, vol. 27, no. 18, pp. 25022–25030, Sep. 2019.
- [36] L. Zhao *et al.*, "Time-stretched femtosecond lidar using microwave photonic signal processing," *J. Lightw. Technol.*, vol. 38, no. 22, pp. 6265–6271, Nov. 2020.
- [37] S. Meyer, J. Squier, and S. Diddams, "Diode-pumped yb: KYW femtosecond laser frequency comb with stabilized carrier-envelope offset frequency," *Eur. Phys. J. D*, vol. 48, pp. 19–26, Jan. 2008.
- [38] T. Yu *et al.*, "Precise and long-term stabilization of the carrier-envelope phase of femtosecond laser pulses using an enhanced direct locking technique," *Opt. Exp.*, vol. 15, no. 13, pp. 8203–8211, Jun. 2007.
- [39] S. Hakobyan, V. Wittwer, K. Gürel, A. Mayer, S. Schilt, and T. Südmeyer, "Carrier-envelope offset stabilization of a GHz repetition rate femtosecond laser using opto-optical modulation of a SESAM," *Opt. Lett.*, vol. 42, no. 22, pp. 4651–4654, Nov. 2017.
- [40] D. Jones *et al.*, "Carrier-envelope phase control of femtosecond mode-locked lasers and direct optical frequency synthesis," *Science*, vol. 288, pp. 635–639, Apr. 2000.
- [41] F. Tauser and A. Leitenstorfer, "Amplified femtosecond pulses from an er: Fiber system: Nonlinear pulse shortening and self-referencing detection of the carrier-envelope phase evolution," *Opt. Exp.*, vol. 11, no. 6, pp. 594–600, Mar. 2003.
- [42] M. Takeda, H. Ina, and S. Kobayashi, "Fourier-transform method of fringe-pattern analysis for computer-based topography and interferometer," *J. Opt. Soc. Amer.*, vol. 72, no. 1, pp. 156–160, Jan. 1982.
- [43] H. Xia and J. Yao, "Characterization of subpicosecond pulses based on temporal interferometry with real-time tracking of higher order dispersion and optical time delay," *J. Lightw. Technol.*, vol. 27, no. 22, pp. 5029–5037, Nov. 2009.